Molecular context of Dopa influences adhesion of mussel-inspired peptides

George D. Degen,^{1†} Keila C. Cunha,^{2†} Zachary A. Levine,^{6,7} J. Herbert Waite,^{2,3,4} Joan-Emma Shea*^{2,5}

¹Department of Chemical Engineering. University of California, Santa Barbara. Santa Barbara, CA, USA.

²Department of Chemistry and Biochemistry. University of California, Santa Barbara. Santa Barbara, CA, USA.

³Department of Molecular, Cellular, and Developmental Biology. University of California, Santa Barbara. Santa Barbara, CA, USA.

⁴Marine Science Institute. University of California, Santa Barbara. Santa Barbara, CA, USA.

⁵Department of Physics. University of California, Santa Barbara. Santa Barbara, CA, USA.

⁶Department of Pathology. Yale School of Medicine. New Haven, CT. USA.

⁷Department of Molecular Biophysics and Biochemistry. Yale University. New Haven, CT, USA.

KEYWORDS. bio-inspired, adhesion, peptides, replica-exchange molecular dynamics, umbrella sampling

ABSTRACT Improving adhesives for wet surfaces is an ongoing challenge. While the adhesive proteins of marine mussels have inspired many synthetic wet adhesives, the mechanisms of mussel adhesion are still not fully understood. Using surface forces apparatus (SFA) measurements and replica-exchange and umbrella-sampling molecular dynamics simulations, we probed the relationships between the sequence, structure, and adhesion of mussel-inspired peptides. Experimental and computational results reveal that peptides derived from mussel foot protein 3 slow (mfp-3s) containing 3,4-dihydroxyphenylalanine (Dopa), a post-translationally modified variant of tyrosine commonly found in mussel foot proteins, form adhesive monolayers on mica. In contrast, peptides with tyrosine adsorb as weakly adhesive clusters. We further considered simulations of mfp-3s derivatives on a range of hydrophobic and hydrophilic organic and inorganic surfaces (including silica, self-assembled monolayers, and a lipid bilayer), and demonstrated that the chemical character of the target surface and proximity of cationic and hydrophobic residues to Dopa affect peptide adsorption and adhesion. Collectively, our results suggest that conversion of tyrosine to Dopa in hydrophobic, sparsely charged peptides influences peptide self-association and ultimately dictates their adhesive performance.

INTRODUCTION

Aqueous electrolyte solutions are challenging environments for adhesives. Nevertheless, marine mussels fasten themselves to surfaces under water using adhesive proteins.¹ The most adhesive mussel foot proteins (mfps) are rich in the catecholic amino acid 3,4-dihydroxyphenylalanine (Dopa),^{2,3} which is derived from tyrosine by post-translational

modification. Dopa has been shown to facilitate adhesion through diverse intermolecular interactions.⁴ As a result, Dopa and other catechols have been incorporated into many synthetic wet adhesives.^{5–8}

Despite the widespread interest in polyphenolic adhesives, the adhesion mechanisms of these materials are not fully understood. Recent research suggests that the adhesion of catechols can be enhanced by neighboring cationic functionalities,9 which may explain the frequent pairing of Dopa and lysine in the adhesive proteins of at least genera of mussels. 10,11 However, while many studies demonstrate binding synergy between catecholic and cationic functionalities,9,12-20 others find that pairing these functionalities yields no increase in catechol-mediated adhesion,21-23 or even decreases adhesion. Furthermore, although Dopa is thought to contribute to mussel adhesion by forming hydrogen bonds with surfaces,26-28 some simulations of mussel-inspired peptides show few hydrogen bonds between Dopa and mica,29,30 a model mineral surface. Consistent with these findings, recent studies suggest that Dopa does not always directly participate in adhesion. Instead, Dopa and other aromatic residues may enhance electrostatic interactions between charged residues and surfaces. 30,31 The disparate proposed roles for Dopa in wet adhesion results highlight the importance of understanding molecular adhesion mechanisms for the rational design of mussel-inspired adhesives.

Simulations have been increasingly used to investigate the conformations and adhesion mechanisms of catecholic materials.^{29,30,32–35} Because most of the characterization of the adhesion of mussel proteins has been performed with a surface forces apparatus (SFA), comparing simulations to complementary SFA experiments is desirable, yet few such studies have been reported.^{29,33} Furthermore, while most studies of mussel-inspired adhesion investigate materials that are highly charged and hydrophilic, a prominent mussel foot protein, mfp-3 *slow* (mfp-3s),

contains few positive charges and is relatively hydrophobic.³⁶ Only half of the many tyrosine residues in mfp-3s are converted to Dopa, in contrast with the extensive modification of tyrosine to Dopa in other mussel foot proteins.^{10,37} Understanding the effect of conversion of tyrosine to Dopa in sparsely charged, hydrophobic materials remains an open research area.

Here, we use force measurements and simulations to investigate binding mechanisms of peptide derivatives of mfp-3s. Adhesion measurements conducted with a surface forces apparatus demonstrate that peptides containing Dopa adsorb into adhesive monolayers on mica in an aqueous electrolyte solution, while peptides containing tyrosine adsorb in weakly adhesive clusters. Molecular dynamics simulations highlight the importance of positive charges for peptide adsorption to mica. Simulations of mfp-3s peptide adsorption on silica, self-assembled monolayers, and a lipid bilayer, coupled with the experimental and computational results on mica surfaces, collectively suggest that the molecular context of Dopa—the nature of the surrounding residues and the target surface—dictates adsorption and adhesion, with implications for the design of mussel-inspired adhesives.

MATERIALS AND METHODS

Surface Forces Apparatus Adhesion Measurements: A previously designed³⁸ peptide derivative of the mussel foot protein 3 slow (mfp-3s), was commercially ordered with unmodified termini (GenScript). Tyrosine residues were enzymatically modified to Dopa using mushroom tyrosinase.³⁹ Peptides containing tyrosine and Dopa were denoted mfp-3s-pep-Tyr and mfp-3s-pep-Dopa, respectively (Figure 1A). Adhesion measurements were performed with a surface forces apparatus (SFA2000, SurForce LLC). In the SFA, mica surfaces were arranged in a crossed-cylinder geometry (Figure 1B), locally equivalent to a sphere of radius *R* contacting a flat surface.⁴⁰ One of the cylinders was mounted on a double cantilever spring of known spring

constant. Translation of the base of the spring at constant velocity (2–12 nm/s) allowed the surfaces to be brought into contact, compressed, and separated. Distance between the mica surfaces was measured with white light multiple beam interferometry. Normal forces between the surfaces were measured with the double cantilever spring and normalized by the average radius of curvature R of the surfaces. Experiments were conducted with a capillary meniscus of peptide solution (250 mM KNO₃, 100 mM acetic acid, pH 3) between the surfaces. Solution conditions were chosen to match a previous study of the same peptides.³³ To measure adhesion, the surfaces were compressed to 100 mN/m, After waiting at maximum compression ($t_{dwell} = 10$ s or 60 min), the surfaces were separated. The tensile force F_{ad} before the surfaces jumped out of contact was converted into an adhesion energy per area between flat surfaces according to the DMT theory, $t_{ad} = -F_{ad}/2\pi R$. Additional details of surface preparation, SFA operation, and the DMT theory are included in the Supporting Information S1.

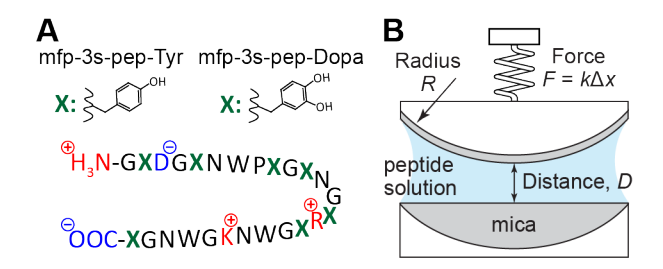


Figure 1. (A) The sequence of the mussel-derived peptides used in this work. The letter X represents either the tyrosine residues in mfp-3s-pep-Tyr or the Dopa residues in mfp-3s-pep-Dopa. (B) Schematic of the surface forces apparatus crossed cylinder configuration.

Molecular Dynamics Simulations—System Parameters, Structures, and Equilibration: Each system consisted of a peptide molecule in a cubic simulation box $(5.2 \times 5.2 \times 5.$

dominant mfp-3s-pep-Dopa states observed in earlier work³³, and Dopa residues were converted back to Tyr residues, when applicable, to create mfp-3s-pep-Tyr structures. The simulations were performed using GROMACS 2018⁴³ and the GROMOS 53A6 force field,⁴⁴ however duplicate simulations were also carried out using the AMBER03* force field for proteins45,46 and TIP3P water⁴⁷ in order to mitigate biases from a single force field. Partial charge assignments for the catechol hydroxyl groups were based on earlier calculations⁴⁸. After solvation, steepest descent energy minimization was carried out for 5,000-100,000 steps, or until a tolerance of 750 kJ/mol/nm was achieved. Simulations were then slowly heated to 300 K for 5 ns using the velocity-rescaling⁴⁹ thermostat and a 1 ps time constant. The positions of heavy atoms in the peptide were initially restrained using a force of 1,000 kJ/mol/nm² in all directions, and under an NVT ensemble with periodic boundary conditions in the x, y and z directions. Peptide hydrogen bonds were constrained using the LINCS method⁵⁰ while water bonds were constrained using the SETTLE algorithm.⁵¹ A leapfrog algorithm⁵² was also used to integrate the equations of motion with a time step of 2 fs. In addition, Particle Mesh Ewald (PME) summation⁵³ was used to treat long-range electrostatic interactions beyond a cutoff radius of 1.0 nm in Fourier space while short-range electrostatics and van der Waals interactions were tabulated in direct space. A Verlet⁵⁴ cut-off scheme was used for neighbor searching, with non-bonded pairs updated every 10 steps. After temperature and volume equilibration, an unrestrained 20 ns NPT simulation was performed to equilibrate the pressure of the system using a Berendsen barostat⁵⁵ coupled isotropically (in all dimensions) at 1 bar. A time constant of 0.5 ps and isothermal compressibility of 4.5×10^{-5} bar⁻¹ was used in each bulk water simulation.

For systems containing mica, a mica model⁵⁶ consisting of a single layer of $muscovite-2M_1$ (KAl₂(Si₃Al)O₁₀ (OH)₂) was placed in the simulation box and modeled with parameters from the

INTERFACE force field.⁵⁷ The mica surface contained 5,120 atoms and was treated as an infinite molecule than spanned the x- and y-dimensions of the simulation box. During equilibration, heavy atoms were restrained on the surface while light atoms (i.e., hydrogen) were free to move. The negatively charged mica surface was neutralized using 255 K⁺ ions, resulting in a net neutral system. During NPT equilibration, a semi-isotropic Berendsen barostat was used with no compressibility in the x- and y-dimensions and aqueous compressibility (4.5 × 10⁻⁵ bar⁻¹) in the z-dimension to maintain the presence of a surface. Initial peptide structures in the vicinity of mica were taken from the final states deduced from bulk REMD simulations, described in detail below.

Replica-Exchange Molecular Dynamics (REMD) Simulations: The coordinates and velocities obtained from the last frame of each NPT simulation were used to create replicas for each REMD simulation (50 replicas using the GROMOS force field and 70 replicas using the AMBER03* force field). Each replica was heated to a target temperature over 20 ns at constant volume (NVT ensemble). The temperatures ranged roughly from 295–500 K for bulk simulations and 295–470 K for mica-containing simulations. Production REMD simulations were then performed for 400 ns (bulk simulations) or 500 ns (mica simulations) using the Nose-Hoover thermostat⁴⁹ with a 1 ps time constant. The average exchange rate between adjacent replicas was approximately 25%, optimized from the initial 10 ns of the REMD simulation. Exchanges between replicas were attempted every 3 ps. The first 100 ns of the production run was discarded to ensure adequate equilibration of each replica, while the analyses described in this study were limited only to subsequent times in the production run. The cutoff radii used in the simulations were 1.2 nm for the short-range electrostatics and van der Waals interactions.

Umbrella Sampling Simulations: The most dominant structures in REMD simulations were used as the initial peptide structures for umbrella sampling simulations. Peptides bound to mica were then pulled away from or pushed toward the mica to sample both attractive and repulsive potential of mean force (PMF). In instances where the peptide was pulled away from a surface not explored with REMD simulations, the peptide was added to bulk solution at least 1 nm above the new interface and allowed to diffuse and/or bind to the interface for 20 ns, with parameters similar to those described earlier. Upon binding, the peptide was pulled away or pushed toward the surface as described for the mica simulations. Peptides were pulled/pushed with a force of 5000 kJ/mol/nm² at a rate of 1 nm/ns until they traversed a net distance of 2-4 nm. Replicas were tabulated every 0.1 nm, yielding an ensemble of about 20-40 replicas. Following collection of the ensemble, we harmonically constrained the peptide in each position and collected energetics for 70 ns using a Nose-Hoover thermostat⁴⁹ and 1 ps time constant. We utilized the weightedhistogram analysis method (WHAM) to calculate the free energy of adhesion to each interface. A POPC membrane consisting of 512 lipids was also generated for the umbrella sampling simulations using the CHARMM-GUI web interface (http://www.charmm-gui.org), which was equilibrated at 300 K for 100 ns using the AMBER03 force field.

Simulation Analysis Tools: Standard GROMACS tools used for simulation analysis included: gmx cluster, to cluster peptide structures within an empirically-defined RMSD cutoff (typically 1.4 Å) based on non-terminal backbone atoms within the Daura algorithm⁵⁸; gmx hbond, to measure the number of hydrogen bonds within a cutoff distance (donor–acceptor) of 3.5 Å and 30° angle (hydrogen-donor–acceptor); gmx gyrate, to obtain the radius of gyration (R_g); gmx density, to calculate atomic densities; gmx mindist, to measure the number of atoms within a given distance from the surface; gmx do_dssp, to deduce peptide secondary structures through

the DSSP^{59,60} algorithm. Molecular representations were generated by Visual Molecular Dynamics (VMD) 1.9.4.⁶¹

RESULTS AND DISCUSSION

Surface Forces Apparatus Adhesion Measurements of Mfp-3s Peptides on Mica: Presence of Dopa Enables Adsorption of Monolayers. We hypothesized that conversion of tyrosine to Dopa would strengthen adhesion of mfp-3s peptides to mica surfaces. To test this hypothesis, we used a surface forces apparatus to measure adhesion to mica of peptides containing tyrosine (mfp-3spep-Tyr) and peptides with tyrosine converted to Dopa (mfp-3s-pep-Dopa). Figure 2A shows a representative plot of force/radius F/R as a function of distance D between mica surfaces after deposition of mfp-3s-pep-Dopa (blue circles). A plot of forces measured between bare mica surface in salt solution (gray circles) is shown for comparison. The plots demonstrate that Mfp-3s-pep-Dopa readily adsorbed into adhesive films on mica. In salt solution, the mica surfaces are slightly adhesive (adhesion force 3.0 ± 0.3 mN/m), consistent with previous measurements of forces between mica surfaces in a similar solution.¹⁶ Adhesion between mica surfaces in acidic monovalent electrolyte solutions is enabled by hydronium ions replacing hydrated cations on the mica surface, resulting in decreased hydration repulsion and increased van der Waals attraction.⁶² After deposition of mfp-3s-pep-Dopa at approximate peptide concentration 5 μ M, the adhesion force increased to $-F_{ad}/R = 11.0 \pm 0.3$ mN/m ($E_{ad} = 1.8$ mJ/m²). Increasing the concentration of mfp-3s-pep-Dopa to 10 μ M further increased the adhesion force to 17 \pm 6 mN/m (2.7 mJ/m²). The adhesion force was constant over consecutive measurements and was independent of the separation velocity over the range of velocities tested here (Figure S1), indicating that adhesion resulted from short-ranged non-covalent interactions.

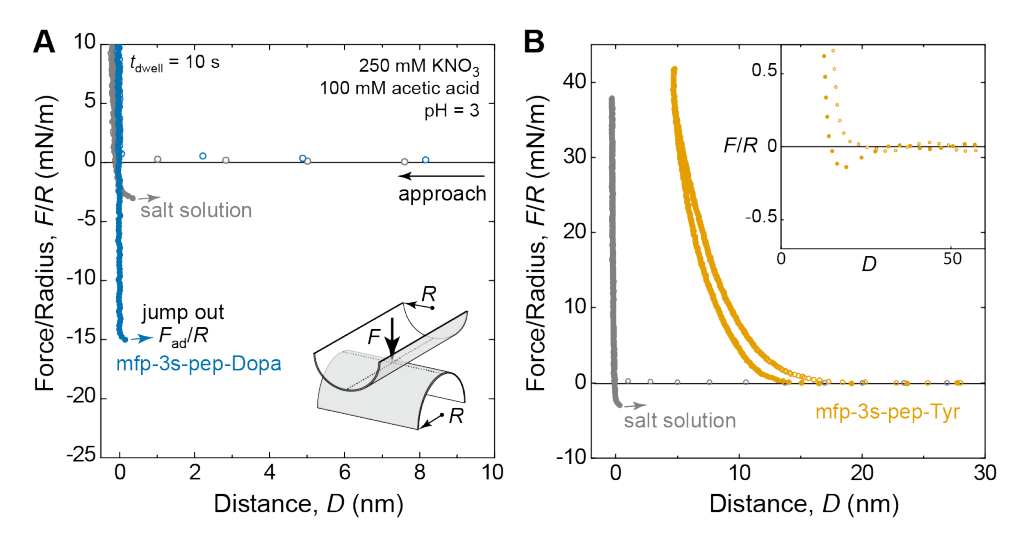


Figure 2. (A) Plot of force/radius F/R vs. mica separation distance D for bare mica surfaces in salt solution (gray circles), and for mica surfaces after deposition of mfp-3s-pep-Dopa (blue circles). (B) Force-distance plots for mica surfaces after deposition of mfp-3s-pep-Tyr (orange circles). Inset shows weak adhesion of the adsorbed cluster. Open circles correspond to compression of the surfaces; closed circles correspond to separation.

The film thickness after deposition of mfp-3s-pep-Dopa (-0.2 ± 0.4 nm) was not significantly different from the thickness measured in salt solution (0.1 ± 0.3 nm), suggesting that monolayers of peptide adsorbed onto each mica surface. The possibility of measuring negative values of film thickness is a consequence of the experimental procedure, described in the Supporting Information S1. At the solution conditions used in this work, adsorbed potassium ions populate the negatively charged mica lattice. The diameter of a hydrated potassium ion is 6.6 Å.⁴⁰ The cross-sectional diameter of mfp-3s-pep-Dopa was estimated as 7 Å, the approximate diameter of a tyrosine amino acid.⁶³ Replacing hydrated potassium ions with a monolayer of peptide is expected to minimally change the film thickness, whereas a multilayer would increase the film thickness. Therefore, the increase in adhesion force without change in film thickness after deposition of peptides is consistent with adsorption of a monolayer on each surface. The further

increase in adhesion force and unchanging film thickness upon increasing the peptide concentration suggests that the monolayer is incomplete and can accommodate additional peptides without forming a multilayer. With incomplete monolayers on each surface, adhesion forces likely result from bridging interactions in which individual peptide molecules bind to both mica surfaces.⁶⁴ The adhesion also depended on the dwell time in contact and the time since incubation (Figure S2), consistent with changes in the number or distribution of bridging interactions of peptides, discussed in the Supporting Information S2.

In contrast with mfp-3s-pep-Dopa, mfp-3s-pep-Tyr did not form adhesive monolayers on mica. Instead, for some contact locations between the mica surfaces, no evidence of peptide adsorption was observed, with the adhesion force and film thickness remaining the same as the values measured in salt solution. At other contact points, long-ranged repulsion (5–30 nm) and minimal adhesion were measured (Figure 2B). This behavior was attributed to association of the peptides in solution and subsequent heterogeneous adsorption of associated assemblies on the mica. Consequently, contact between the surfaces either results in compression of one or more assemblies, or contact between bare mica surfaces. Peptide association was corroborated by dynamic light scattering measurements of the mfp-3s-pep-Tyr solution that revealed particles of diameter 200–300 nm (Figure S3). These findings are consistent with a previous study³⁸ that reported coacervation of the same peptide in acidic aqueous solution, albeit at higher ionic strength than used here.

Replica-Exchange Molecular Dynamics Simulations of Mfp-3s Peptides on Mica: Molecular Insights into the Conformation and Binding of Dopa and Tyr Variants. To explore the impact of hydroxylation of tyrosine to Dopa on peptide structure and adhesion, we performed replicaexchange molecular dynamics (REMD) simulations using the GROMOS force field. Individual

molecules of mfp-3s-pep-Tyr and mfp-3s-pep-Dopa were simulated in bulk water and in the presence of mica. Figure 3A-B (left) depicts representative structures and associated probabilities of the three most probable peptide conformations in bulk water. Figure 3 (right) shows plots of the peptide radius of gyration (R_g) versus end-to-end distance (R_{ee}). The dominant conformations present β -sheets and interactions between pairs of aromatic residues (Trp, Tyr and Dopa) or interactions between an aromatic residue and a charged residue (Arg, Lys and the N-terminal Gly). Small values of both R_g and R_{ee} correspond to compact structures, while larger values of R_g and R_{ee} indicate extended structures. Large R_g and small R_{ee} indicates an extended structure with a beta-hairpin that places the termini close to each other. Mfp-3s-pep-Tyr adopted both extended and compact structures in solution, whereas the mfp-3s-pep-Dopa adopted mostly extended states. Mfp-3s-pep-Dopa was also more solvent-exposed and formed more hydrogen bonds with water compared with mfp-3s-pep-Tyr (Figure S4), consistent with the second hydroxyl group on each of the seven Dopa residues.

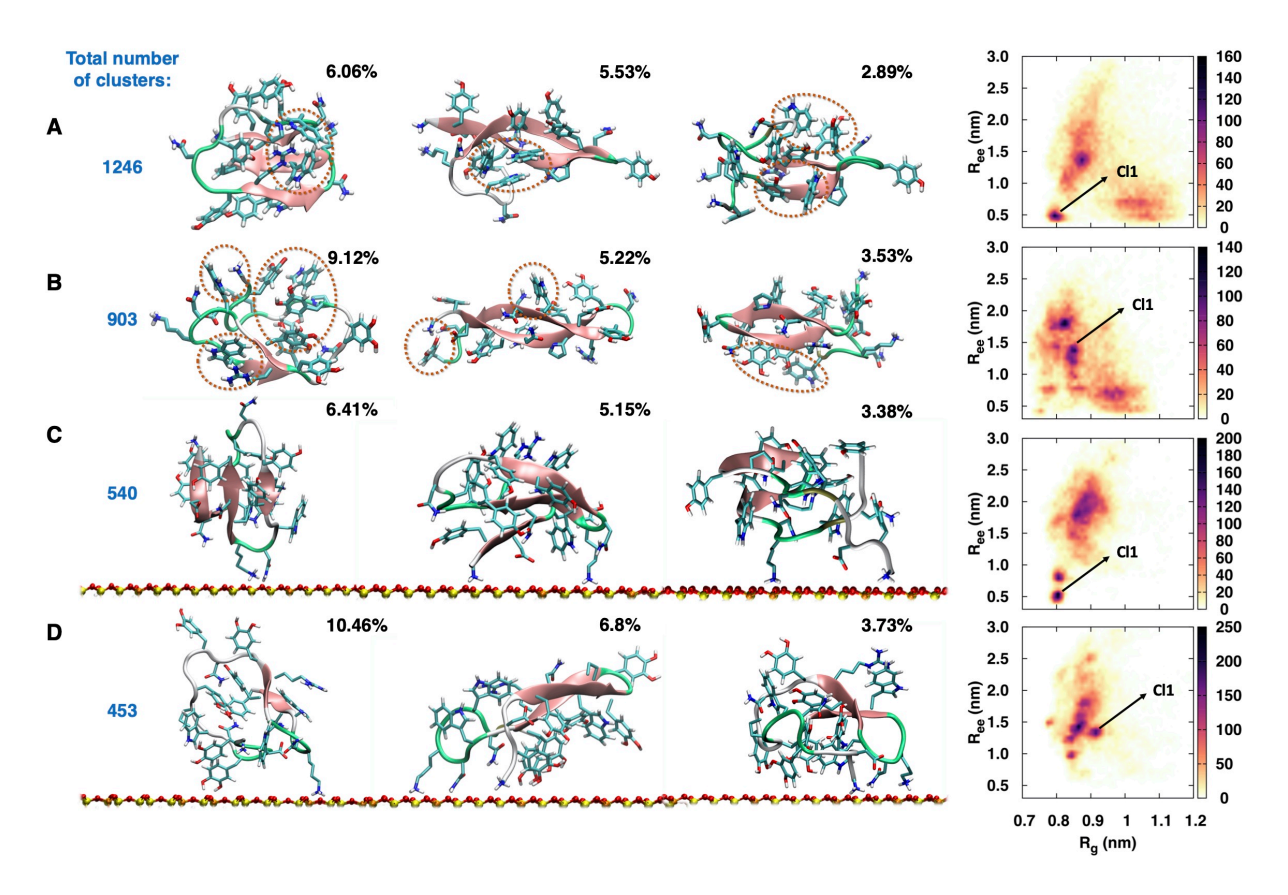


Figure 3. Top three clusters of likely conformations (*left*) and end-to-end distance R_{ee} vs radius of gyration R_g (*right*) for (A) mfp-3s-pep-Tyr and (B) mfp-3s-pep-Dopa in bulk water and (C) mfp-3s-pep-Tyr and (D) mfp-3s-pep-Dopa in the presence of mica. The dashed ovals in the cartoon representations of the peptides indicate interactions between aromatic groups or between aromatic and charged groups. Arrows in the plots of R_{ee} vs. R_g indicate the most probable cluster.

In the presence of a mica surface, both peptides lost secondary structure. The three most likely conformations from GROMOS53a6 are shown in Figure 3C-D. The probability of adopting β -sheets decreased and the probability of adopting random coils increased relative to the probabilities in bulk solution (Figures S5 and S6), commensurate with a decrease in water solvation (Figure S4). Adsorption to mica decreased the number of intramolecular hydrogen bonds in mfp-3s-pep-Tyr (Figure S7), consistent with the loss of β -sheets. In contrast, the

number of intramolecular hydrogen bonds within mfp-3s-pep-Dopa was not significantly affected by adsorption. On mica, mfp-3s-pep-Tyr adopted more compact structures than in solution, while mfp-3s-pep-Dopa sampled structures with larger $R_{\rm g}$ and better spreading over the surface, as indicated by the radius of gyration in the xy-plane parallel to the interface, $R_{\rm g}(z)$, which corresponds to the ability of the peptide to splay along the surface of mica (Figure 4A). We note that direct corroboration of the different conformations of adsorbed mfp-3s-pep-Tyr and mfp-3s-pep-Dopa with SFA measurements was precluded by the aggregation of mfp-3s-pep-Tyr.

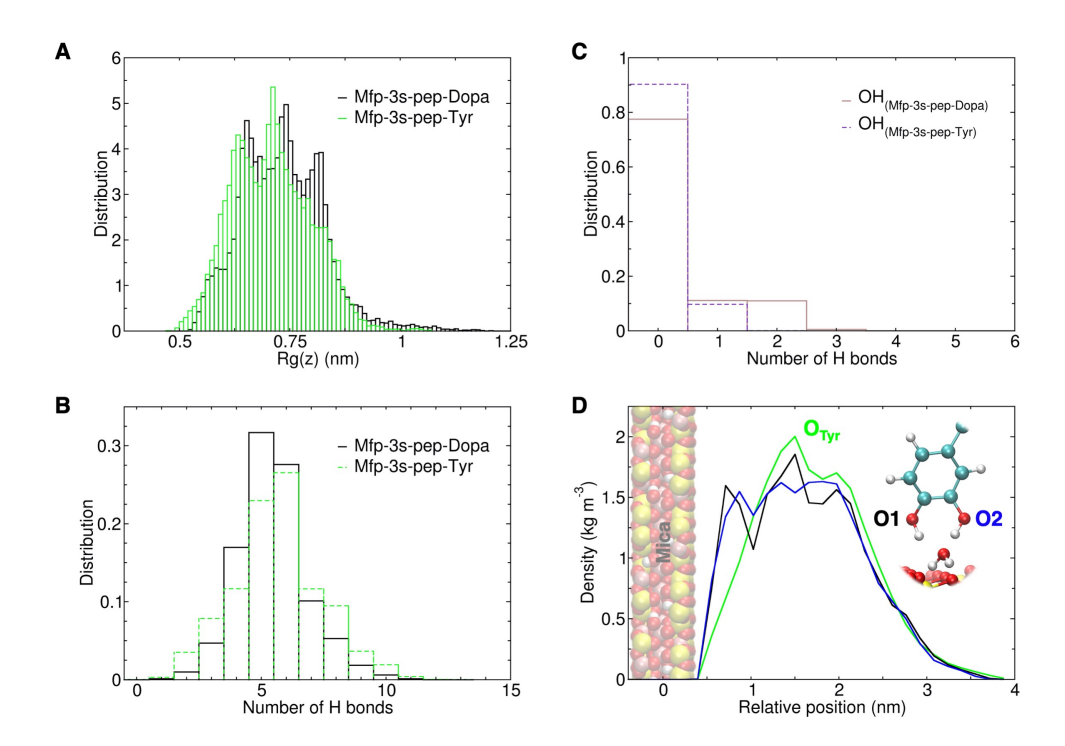


Figure 4. (A) Histogram of the radius of gyration about the *z*-axis for each peptide (B) Normalized histogram of the number of hydrogen bonds between each peptide and the mica surface. (C) Histogram of the number of hydrogen bonds between dopa and Tyr hydroxyls and mica. (D) Density distribution along the *z*-axis of the oxygen atoms from tyrosine and Dopa hydroxyls.

Interactions between both peptides and the mica surface involved the formation of hydrogen bonds. Mfp-3s-pep-Tyr and mfp-3s-pep-Dopa formed similar numbers of hydrogen bonds with mica (Figure 4B). To identify the residues responsible for the hydrogen bonding in each peptide, we calculated the number of hydrogen bonds formed between each residue type and mica (Figures S8 and S9). Positively charged residues (Lys, Arg, and the N-terminal Gly) formed most of the hydrogen bonds with mica. For both peptides, lysine formed an average of 2.4 hydrogen bonds with mica, indicating that lysine often binds to the surface with all three hydrogens on its pendant amine. The cationic N-terminal glycine of mfp-3s-pep-Tyr and mfp-3spep-Dopa formed 2.3 and 1.8 hydrogen bonds, respectively. Arginine formed fewer hydrogen bonds with mica (0.2-0.4 avg). Uncharged residues including Dopa (0.3 avg) and Asparagine (0.5-0.7 avg) formed few hydrogen bonds with mica (Figure 4C and S8). However, 83% of the structures from the most sampled cluster of mfp-3s-pep-Dopa involved bidentate hydrogen bonding between the hydroxyls of Dopa and mica, (Figure 3D). Even after driving the peptide onto the surface to emulate the compression associated with SFA experiments, a single Dopa residue remained stably bound (Figure S10, Supporting Information S3). Nevertheless, Dopa localized at the mica surface much more than Tyr, as shown by the density of hydroxyl oxygens along the z-axis (normal to the mica surface) (Figure 4D), possibly corresponding to the formation of outersphere complexes between Dopa and bound water.³⁸ This result is also confirmed by the overall minimum distances between the hydroxyl oxygens of Dopa and the mica surface (Figure S11), and by the greater probability of finding two or more Dopa residues near mica compared with Tyr (Figure S12). We also observed correlations between the positions of Dopa and charged residues. The radial distribution function of NH₃⁺ atoms around Dopa or Tyr aromatic rings in peptides exposed to a mica surface (Figure S13) shows that the density of NH₃⁺ is higher within 4 Å of Dopa than within the same distance of Tyr. Whether the proximity results from interactions between the residues or cooperative interactions with the mica surface remains to be determined.

Comparing our results to other studies of the adhesion of mussel-inspired peptides yields insights into the influence of Dopa content on adsorption and adhesion. A recent study²⁵ of peptides with similar Dopa content but greater lysine content than mfp-3s-pep-Dopa showed comparable adhesion to our SFA measurements of mfp-3s-pep-Dopa on mica. In that study, replacing Dopa by tyrosine or phenylalanine was shown to increase adhesion, in contrast with our SFA results showing increased adhesion of peptides containing Dopa relative to peptides containing tyrosine. The discrepancy can be explained by considering the relationship between adsorption and adhesion. Highly cationic peptides are favored to adsorb on mica. If a sparse monolayer adsorbs such that individual adhesive molecules can bridge both surfaces, or if a monolayer is deposited onto a single surface, then conversion of tyrosine to Dopa increases adhesion.^{29,64} If a dense monolayer adsorbs on both surfaces, or a multilayer adsorbs on one or both surfaces, then cohesion between the films dictates the measured adhesion force. In that case, conversion of tyrosine to Dopa decreases adhesion due to weakened cation- π interactions.²⁵ Our results demonstrate that the presence of Dopa enables mildly cationic, hydrophobic peptides to adsorb as monolayers, whereas peptides containing tyrosine associate in solution and adsorb in clusters. The differences in adsorption of mfp-3s-pep-Tyr and mfp-3s-pep-Dopa measured in the SFA experiments are consistent with our simulations showing reduced hydration and higher content of beta-sheets in mfp-3s-pep-Tyr relative to mfp-3s-pep-Dopa. These properties might favor association of multiple mfp-3s-pep-Tyr molecules in solution, possibly driven by cation- $\pi^{65,66}$ or π -cation- π^{67} interactions. Our results are also consistent with the association reported for mussel-inspired surface primers¹⁶ and peptides,⁶⁶ and with reports of the impact of molecular structure on association and adhesion of mussel-inspired materials.^{29,35} Ultimately, the influence of Dopa on adhesion depends on the molecular context, including the density and thickness of the adsorbed adhesive and the balance between adhesion and cohesion. Our results indicate that the propensity of an adhesive to aggregate is another key determinant of the impact of Dopa on adhesion.

Effect of Surface Hydrophobicity on Mfp-3s Peptide Binding: Replica-Exchange and Umbrella Sampling MD Simulations. The chemical character of the target surface is expected to influence peptide adhesion. We performed AMBER03* REMD simulations to compare the effects of hydrophilic and hydrophobic surfaces on peptide secondary structure. We first replicated the GROMOS53a6 REMD simulations by simulating the peptides in bulk water and on mica using the AMBER03* model (Figure S14). We observed qualitatively similar, but slightly more disordered monomer conformations compared with the GROMOS simulations. Hydrophilic surfaces including silica (Figure S15, left) and hydrophilic self-assembled monolayers (SAMs) (Figure S15, right) result in peptides that remain globular. In contrast, hydrophobic SAMs (Figure S15, middle) result in heavily splayed peptides on the surface. These results demonstrate that surface hydrophobicity strongly influences the conformation of bound peptides.

To further explore the interactions between the mussel-inspired peptides and various surfaces, we calculated peptide adhesion to mica and additional inorganic and organic surfaces using umbrella sampling simulations. Our AMBER03* model shows that mfp-3s-pep-Tyr and mfp-3s-pep-Dopa bind with similar energy to mica (Figure S16, *top*), whereas on silica, mfp-3s-pep-Dopa is 50% more adhesive than mfp-3s-pep-Tyr (Figure S16, *second row*). Like the adhesion to mica, the adhesion of mfp-3s-pep-Tyr to a hydrophilic SAM (Figure S16, *third row*) matched the

previously reported adhesion of mfp-3s-pep-Dopa to the same SAM.³³ The simulated adhesion of mfp-3s-pep-Dopa to a hydrophobic SAM in the same study was 250% larger than the adhesion of mfp-3s-pep-Tyr reported here (Figure S16, third row). Mfp-3s-pep-Dopa also bound to lipid (POPC) membranes (Figure S16, fourth row) with adhesion between the values for hydrophobic and hydrophilic SAMs. Our results and previous simulations and SFA adhesion measurements³³ demonstrate that mfp-3s-pep-Tyr and mfp-3s-pep-Dopa bind more strongly to hydrophobic surfaces than to hydrophilic surfaces. The greater adhesion to hydrophobic surfaces may result from hydrophobic interactions between the peptides and the surface. Hydrophobic surfaces may also promote adhesion by disrupting the water layers that coat hydrophilic surfaces and discourage adhesion.³⁸ Regardless of the origin, the enhanced adhesion of peptides to hydrophobic surfaces may also account for the structural changes of peptides exposed to hydrophobic surfaces (described above). The results also indicate that the effect of hydroxylation of Tyr to Dopa on peptide adhesion depends on the chemical character of the surface. Interestingly, hydroxylation increases adhesion to silica, but not other hydrophilic surfaces (mica and hydrophilic SAMs), suggesting that the adhesion of polyphenolic peptides depends on factors beyond surface hydrophobicity such as charge density and counterion arrangement, density and organization of hydrogen bonding groups, and thermal mobility of surface groups.

Umbrella Sampling Simulations of Short, Palindromic Peptides: Effect of Hydroxylation and Position of Aromatic Groups on Adhesion. To evaluate the relationships between hydroxylation of aromatic groups, proximity of those groups to other residues, and adhesion to mica, we performed umbrella sampling simulations of short, palindromic peptides under identical conditions to the umbrella sampling simulations of mfp-3s peptides. We investigated the following peptides: P1 (XKGGGKX), P2 (XGKGKGX), and P3 (XWKGKWX), where X

denotes an aromatic residue, either Phe (no hydroxyls), Tyr (one hydroxyl), or Dopa (two hydroxyls), nine peptides in total. Dopa and Lysine were identified as key amino-acids in our simulations of binding of mpf-3s peptides to mica, and glycine is a staple in mfp sequences that provides flexibility to the peptide chain. The peptides were designed to test the influences of hydroxylation and molecular context of binding groups on adhesion of a peptide with minimal sequence complexity. P1 contained an aromatic residue adjacent to Lys, while P2 and P3 incorporated an amino acid spacer (Gly for P2, Trp for P3) between aromatic residues and lysine. Umbrella sampling simulations of each peptide (Figure 5) reveal that when Lys is adjacent to an aromatic group (P1), peptide adhesion to mica increases with increasing hydroxylation of aromatic groups, with P1-Dopa peptides exhibiting a more negative potential of mean force than P1-Tyr and P1-Phe. In peptides where Lys is separated from an aromatic group by a Gly residue (P2), P2-Dopa and P2-Tyr yield equivalent adhesion and outperform P2-Phe. In peptides where Lys is separated from an aromatic group by a Trp residue (P3), we find that P3-Dopa adheres less strongly than P3-Tyr and P3-Phe. Interestingly, proximity of hydrophobic and residues to cationic residues has been recently shown to favor cation-π interactions, 66 suggesting that hydrophobic residues may enhance cohesion at the expense of adhesion. Ultimately, our results indicate that while Tyr-containing peptides tend to outperform Phe-containing peptides, the adhesive performance of Dopa relative to Tyr and Phe is influenced by proximity to charged and hydrophobic residues.

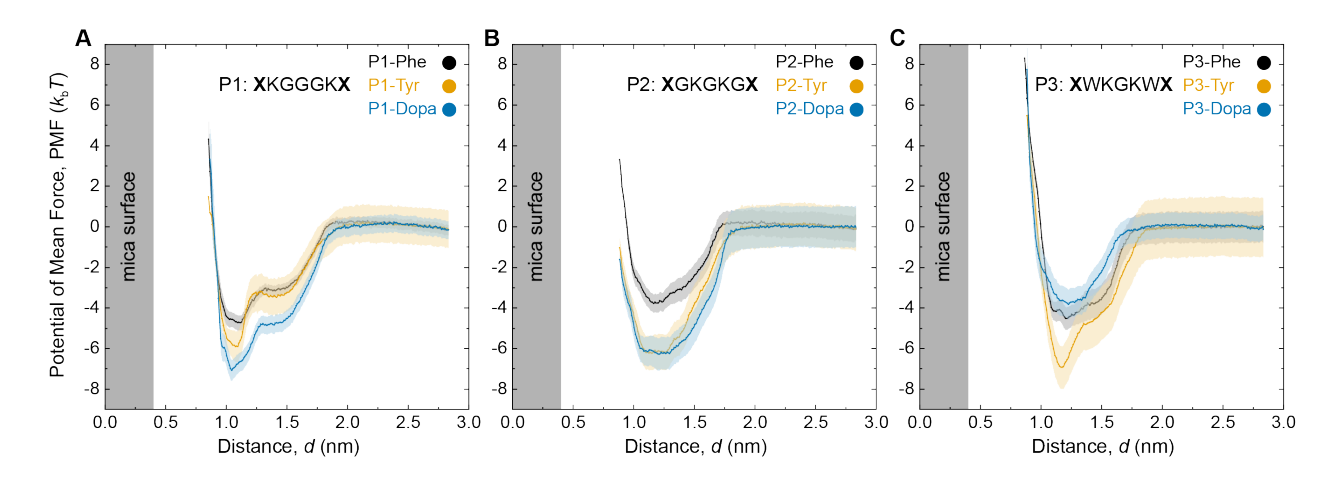


Figure 5. Plots of potential of mean force (PMF) vs. distance *d* from a mica surface calculated from umbrella sampling simulations of aromatic peptides. We investigated the following peptides: (A) P1, sequence XKGGGKX; (B) P2, sequence XGKGKGX; and (C) P3, sequence XWKGKWX. The letter X denotes an aromatic residue containing either no hydroxyls (Phe), one hydroxyl (Tyr), or two hydroxyls (Dopa).

CONCLUSIONS

We investigated three aspects of the molecular context of Dopa in mussel-inspired peptides: the tendency of the peptide to aggregate, the chemical character of the target surface, and the proximity of neighboring charged and aromatic groups. We demonstrated that sparsely charged, hydrophobic peptides containing Dopa form adhesive monolayers on mica, while peptides containing tyrosine associate in solution and adsorb in clusters. Atomistic molecular simulations revealed that positively charged residues drive adsorption onto mica through direct interactions with the surface. While we did not observe extensive hydrogen bonding between Dopa and mica, Dopa hydroxyls were more localized at the mica surface than Tyr hydroxyls. For surfaces other than mica, simulations show that hydrophobicity strongly influences peptide conformation, but that adhesion cannot be predicted from hydrophobicity alone. Simulations also showed that when the aromatic group is separated from Lys, peptides containing Dopa bind no more strongly to

mica than peptides containing Tyr, and in some cases bind less strongly. Our results highlight ways in which the molecular context of Dopa influences peptide association, adsorption, and adhesion. By exploring the roles of Dopa and other amino acids in peptide adhesion, this work clarifies the relationships between peptide structure, surface chemistry, and adhesive performance to enable rational design of mussel-inspired adhesives.

ASSOCIATED CONTENT

Supporting Information. SFA Experimental Details; SFA Time Dependence; Simulation Details.

AUTHOR INFORMATION

Corresponding Author

*Joan-Emma Shea – Department of Chemistry and Biochemistry, University of California, Santa Barbara, California 93106, United States; Department of Physics, University of California, Santa Barbara, California 93106, United States; shea@ucsb.edu

Author Contributions

The manuscript was written through contributions of all authors. All authors have given approval to the final version of the manuscript. †These authors contributed equally.

ACKNOWLEDGMENT

G.D.D. was supported by the National Science Foundation Graduate Research Fellowship Program under Grant No. 1650114. Computational support from the Extreme Science and Engineering Discovery Environment (XSEDE) through National Science Foundation (NSF) grant number TG-MCA05S027 is acknowledged. All the simulations have been performed on the Stampede 2 supercomputer at the Texas Advanced Computing Center at the University of Texas at Austin. J.-E.S. acknowledges the support from the National Science Foundation (NSF)

Grant MCB-1716956). The research reported here was supported by the National Science Foundation (NSF) Materials Research Science and Engineering Center (MRSEC) at UC Santa Barbara (NSF DMR 1720256) through IRG–3. The UC Santa Barbara MRSEC is a member of the Materials Research Facilities Network (https://mrfn.org).

ABBREVIATIONS

mfp, mussel foot protein; SFA, surface forces apparatus; REMD, replica-exchange molecular dynamics; SAM, self-assembled monolayer.

REFERENCES

- (1) Waite, J. H. Mussel Adhesion Essential Footwork. *J. Exp. Biol.* **2017**, 220 (4), 517–530.
- (2) Danner, E. W.; Kan, Y.; Hammer, M. U.; Israelachvili, J. N.; Waite, J. H. Adhesion of Mussel Foot Protein Mefp-5 to Mica: An Underwater Superglue. *Biochemistry* **2012**, *51* (33), 6511–6518.
- (3) Lin, Q.; Gourdon, D.; Sun, C.; Holten-Andersen, N.; Anderson, T. H.; Waite, J. H.; Israelachvili, J. N. Adhesion Mechanisms of the Mussel Foot Proteins Mfp-1 and Mfp-3. *Proc. Natl. Acad. Sci. U. S. A.* **2007**, *104* (10), 3782–3786.
- (4) Li, Y.; Cao, Y. The Molecular Mechanisms Underlying Mussel Adhesion. *Nanoscale Adv.*2019, 1 (11), 4246–4257.
- (5) Lee, B. P.; Messersmith, P. B.; Israelachvili, J. N.; Waite, J. H. Mussel-Inspired Adhesives and Coatings. *Annu. Rev. Mater. Res.* **2011**, *41* (1), 99–132.
- (6) Kord Forooshani, P.; Lee, B. P. Recent Approaches in Designing Bioadhesive Materials Inspired by Mussel Adhesive Protein. *Journal of Polymer Science, Part A: Polymer Chemistry*. John Wiley and Sons Inc. January 1, 2017, pp 9–33.

- (7) Zhang, W.; Wang, R.; Sun, Z. M.; Zhu, X.; Zhao, Q.; Zhang, T.; Cholewinski, A.; Yang, F.; Zhao, B.; Pinnaratip, R.; Forooshani, P. K.; Lee, B. P. Catechol-Functionalized Hydrogels: Biomimetic Design, Adhesion Mechanism, and Biomedical Applications. *Chemical Society Reviews*. Royal Society of Chemistry January 21, 2020, pp 433–464.
- (8) Guo, Q.; Chen, J.; Wang, J.; Zeng, H.; Yu, J. Recent Progress in Synthesis and Application of Mussel-Inspired Adhesives. *Nanoscale* **2020**, *12* (3), 1307–1324.
- (9) Maier, G. P.; Rapp, M. V; Waite, J. H.; Israelachvili, J. N.; Butler, A. Adaptive Synergy between Catechol and Lysine Promotes Wet Adhesion by Surface Salt Displacement. *Science* **2015**, *349* (6248), 625–628.
- (10) Waite, J. H.; Qin, X. Polyphosphoprotein from the Adhesive Pads of Mytilus Edulis. Biochemistry 2001, 40 (9), 2887–2893.
- (11) Petrone, L.; Kumar, A.; Sutanto, C. N.; Patil, N. J.; Kannan, S.; Palaniappan, A.; Amini, S.; Zappone, B.; Verma, C.; Miserez, A. Mussel Adhesion Is Dictated by Time-Regulated Secretion and Molecular Conformation of Mussel Adhesive Proteins. *Nat. Commun.* 2015, 6 (4), 8737.
- (12) Rapp, M. V; Maier, G. P.; Dobbs, H. A.; Higdon, N. J.; Waite, J. H.; Butler, A.; Israelachvili, J. N. Defining the Catechol-Cation Synergy for Enhanced Wet Adhesion to Mineral Surfaces. J. Am. Chem. Soc. 2016, 138 (29), 9013–9016.
- (13) Li, Y.; Wang, T.; Xia, L.; Wang, L.; Qin, M.; Li, Y.; Wang, W.; Cao, Y. Single Molecule Study of the Synergistic Effects of Positive Charges and Dopa for Wet Adhesion. *J. Mater. Chem. B* **2017**, *5*, 4416–4420.

- (14) Li, Y.; Liang, C.; Gao, L.; Li, S.; Zhang, Y.; Zhang, J.; Cao, Y. Hidden Complexity of Synergistic Roles of Dopa and Lysine for Strong Wet Adhesion. *Mater. Chem. Front.*2017, 1 (12), 2664–2668.
- (15) Han, L.; Gong, L.; Chen, J.; Zhang, J.; Xiang, L.; Zhang, L.; Wang, Q.; Yan, B.; Zeng, H. Universal Mussel-Inspired Ultrastable Surface-Anchoring Strategy via Adaptive Synergy of Catechol and Cations. *ACS Appl. Mater. Interfaces* **2018**, *10* (2), 2166–2173.
- (16) Degen, G. D.; Stow, P. R.; Lewis, R. B.; Andresen Eguiluz, R. C.; Valois, E.; Kristiansen, K.; Butler, A.; Israelachvili, J. N. Impact of Molecular Architecture and Adsorption Density on Adhesion of Mussel-Inspired Surface Primers with Catechol-Cation Synergy. J. Am. Chem. Soc. 2019, 141 (47), 18673–18681.
- (17) Shin, M.; Shin, J. Y.; Kim, K.; Yang, B.; Han, J. W.; Kim, N. K.; Cha, H. J. The Position of Lysine Controls the Catechol-Mediated Surface Adhesion and Cohesion in Underwater Mussel Adhesion. *J. Colloid Interface Sci.* **2020**, *563*, 168–176.
- (18) Mu, Y.; Mu, P.; Wu, X.; Wan, X. The Two Facets of the Synergic Effect of Amine Cation and Catechol on the Adhesion of Catechol in Underwater Conditions. *Appl. Surf. Sci.* **2020**, *530*, 146973.
- (19) Tiu, B. D. B.; Delparastan, P.; Ney, M. R.; Gerst, M.; Messersmith, P. Cooperativity of Catechols and Amines in High Performance Dry/Wet Adhesives. *Angew. Chemie Int. Ed.* 2020, 59 (38), 16616–16624.
- (20) Li, Y.; Cheng, J.; Delparastan, P.; Wang, H.; Sigg, S. J.; DeFrates, K. G.; Cao, Y.; Messersmith, P. B. Molecular Design Principles of Lysine-DOPA Wet Adhesion. *Nat*.

- Commun. 2020, 11 (1), 1-8.
- (21) Wang, J.; Tahir, M. N.; Kappl, M.; Tremel, W.; Metz, N.; Barz, M.; Theato, P.; Butt, H. J. Influence of Binding-Site Density in Wet Bioadhesion. *Adv. Mater.* **2008**, *20* (20), 3872–3876.
- (22) Narkar, A. R.; Kelley, J. D.; Pinnaratip, R.; Lee, B. P. Effect of Ionic Functional Groups on the Oxidation State and Interfacial Binding Property of Catechol-Based Adhesive. *Biomacromolecules* **2018**, *19* (5), 1416–1424.
- (23) Bilotto, P.; Labate, C.; De Santo, M. P.; Deepankumar, K.; Miserez, A.; Zappone, B. Adhesive Properties of Adsorbed Layers of Two Recombinant Mussel Foot Proteins with Different Levels of DOPA and Tyrosine. *Langmuir* **2019**, *35* (48), 15481–15490.
- (24) Lee, B. P.; Chao, C. Y.; Nelson Nunalee, F.; Motan, E.; Shull, K. R.; Messersmith, P. B. Rapid Gel Formation and Adhesion in Photocurable and Biodegradable Block Copolymers with High DOPA Content. *Macromolecules* **2006**, *39* (5), 1740–1748.
- (25) Gebbie, M. A.; Wei, W.; Schrader, A. M.; Cristiani, T. R.; Dobbs, H. A.; Idso, M.; Chmelka, B. F.; Waite, J. H.; Israelachvili, J. N. Tuning Underwater Adhesion with Cation–π Interactions. *Nat. Chem.* **2017**, *9*, 473–479.
- (26) Anderson, T. H.; Yu, J.; Estrada, A.; Hammer, M. U.; Herbert Waite, J.; Israelachvili, J. N. The Contribution of DOPA to Substrate–Peptide Adhesion and Internal Cohesion of Mussel-Inspired Synthetic Peptide Films. *Adv Funct Mater* 2010, 8 (2023), 4196–4205.
- (27) Yu, J.; Wei, W.; Danner, E.; Israelachvili, J. N.; Herbert Waite, J.; Waite, J. H. Effects of

- Interfacial Redox in Mussel Adhesive Protein Films on Mica. *Adv Mater* **2011**, *23* (20), 2362–2366.
- (28) Yu, J.; Wei, W.; Danner, E.; Ashley, R. K.; Israelachvili, J. N.; Waite, J. H. Mussel Protein Adhesion Depends on Interprotein Thiol-Mediated Redox Modulation. *Nat. Chem. Biol.* **2011**, *7* (9), 588–590.
- (29) Wonderly, W. R.; Cristiani, T. R.; Cunha, K. C.; Degen, G. D.; Shea, J. E.; Waite, J. H. Dueling Backbones: Comparing Peptoid and Peptide Analogues of a Mussel Adhesive Protein. *Macromolecules* **2020**, *53* (16), 6767–6779.
- (30) Ou, X.; Xue, B.; Lao, Y.; Wutthinitikornkit, Y.; Tian, R.; Zou, A.; Yang, L.; Wang, W.; Cao, Y.; Li, J. Structure and Sequence Features of Mussel Adhesive Protein Lead to Its Salt-Tolerant Adhesion Ability. *Sci. Adv.* **2020**, *6* (39), eabb7620.
- (31) Fan, H.; Wang, J.; Tao, Z.; Huang, J.; Rao, P.; Kurokawa, T.; Gong, J. P. Adjacent Cationic–Aromatic Sequences Yield Strong Electrostatic Adhesion of Hydrogels in Seawater. *Nat. Commun.* **2019**, *10* (1), 1–8.
- (32) Kanyalkar, M.; Srivastava, S.; Coutinho, E. Conformation of a Model Peptide of the Tandem Repeat Decapeptide in Mussel Adhesive Protein by NMR and MD Simulations. *Biomaterials* **2002**, *23* (2), 389–396.
- (33) Levine, Z. A.; Rapp, M. V; Wei, W.; Mullen, R. G.; Wu, C.; Zerze, G. H.; Mittal, J.; Waite, J. H.; Israelachvili, J. N.; Shea, J.-E. Surface Force Measurements and Simulations of Mussel-Derived Peptide Adhesives on Wet Organic Surfaces. *Proc. Natl. Acad. Sci. U. S. A.* **2016**, *113* (16), 4332–4337.

- (34) Anand, P. P.; Vardhanan, Y. S. Computational Modelling of Wet Adhesive Mussel Foot Proteins (Bivalvia): Insights into the Evolutionary Convolution in Diverse Perspectives. *Sci. Rep.* **2020**, *10* (1), 1–24.
- (35) Chen, A. B.; Shao, Q.; Hall, C. K. Molecular Simulation Study of 3,4-Dihydroxyphenylalanine in the Context of Underwater Adhesive Design. *J. Chem. Phys.* **2021**, *154* (14), 144702.
- (36) Wei, W.; Yu, J.; Broomell, C.; Israelachvili, J. N.; Waite, J. H. Hydrophobic Enhancement of Dopa-Mediated Adhesion in a Mussel Foot Protein. *J. Am. Chem. Soc.* **2013**, *135* (1), 377–383.
- (37) Papov, V. V.; Diamond, T. V.; Biemann, K.; Waite, J. H. Hydroxyarginine-Containing Polyphenolic Proteins in the Adhesive Plaques of the Marine Mussel Mytilus Edulis. *J. Biol. Chem.* **1995**, 270 (34), 20183–20192.
- (38) Wei, W.; Petrone, L.; Tan, Y.; Cai, H.; Israelachvili, J. N.; Miserez, A.; Waite, J. H. An Underwater Surface-Drying Peptide Inspired by a Mussel Adhesive Protein. *Adv. Funct. Mater.* **2016**, *26* (20), 3496–3507.
- (39) Marumo, K.; Waite, J. H. Optimization of Hydroxylation of Tyrosine and Tyrosine-Containing Peptides by Mushroom Tyrosinase. *Biochim. Biophys. Acta* **1986**, 872, 98–103.
- (40) Israelachvili, J. N. Intermolecular and Surface Forces, 3rd ed.; Academic Press, 2011.
- (41) Derjaguin, B. V.; Muller, V. M.; Toporov, Y. P. Effect of Contact Deformations on the

- Adhesion of Particles. J. Colloid Interface Sci. 1975, 53 (2), 314–326.
- (42) Berendsen, H.J.C., Postma, J.P.M., Van Gunsteren, W.F. and Hermans, J. Interaction
 Models for Water in Relation to Protein Hydration. In *Intermolecular Forces*; Pullman,
 B., Ed.; Reidel Publishing Company: Dordrecht, 1981.
- (43) Van Der Spoel, D.; Lindahl, E.; Hess, B.; Groenhof, G.; Mark, A. E.; Berendsen, H. J. C. GROMACS: Fast, Flexible, and Free. *J. Comput. Chem.* **2005**, *26* (16), 1701–1718.
- (44) Oostenbrink, C.; Villa, A.; Mark, A. E.; Van Gunsteren, W. F. A Biomolecular Force Field Based on the Free Enthalpy of Hydration and Solvation: The GROMOS Force-Field Parameter Sets 53A5 and 53A6. *J. Comput. Chem.* **2004**, 25 (13), 1656–1676.
- (45) Beauchamp, K. A.; Lin, Y. S.; Das, R.; Pande, V. S. Are Protein Force Fields Getting Better? A Systematic Benchmark on 524 Diverse NMR Measurements. *J. Chem. Theory Comput.* **2012**, 8 (4), 1409–1414.
- (46) Wang, J.; Wolf, R. M.; Caldwell, J. W.; Kollman, P. A.; Case, D. A. Development and Testing of a General Amber Force Field. *J. Comput. Chem.* **2004**, 25 (9), 1157–1174.
- (47) Jorgensen, W. L.; Chandrasekhar, J.; Madura, J. D.; Impey, R. W.; Klein, M. L. Comparison of Simple Potential Functions for Simulating Liquid Water. *J. Chem. Phys.* 1983, 79 (2), 926–935.
- (48) Das, S.; Lee, B. H.; Linstadt, R. T. H.; Cunha, K.; Li, Y.; Kaufman, Y.; Levine, Z. A.; Lipshutz, B. H.; Lins, R. D.; Shea, J. E.; Heeger, A. J.; Kollbe Ahn, B. Molecularly Smooth Self-Assembled Monolayer for High-Mobility Organic Field-Effect Transistors.

- Nano Lett. **2016**, 16 (10), 6709–6715.
- (49) Hoover, W. G. Canonical Dynamics: Equilibrium Phase-Space Distributions. *Phys. Rev. A* **1985**, *31* (3), 1695–1697.
- (50) Hess, B.; Bekker, H.; Berendsen, H. J. C.; Fraaije, J. G. E. M. LINCS: A Linear Constraint Solver for Molecular Simulations. *J. Comput. Chem.* **1997**, *18* (12), 1463–1472.
- (51) Miyamoto, S.; Kollman, P. A. Settle: An Analytical Version of the SHAKE and RATTLE Algorithm for Rigid Water Models. *J. Comput. Chem.* **1992**, *13* (8), 952–962.
- (52) Hockney, R. W. The Potential Calculation and Some Applications. In *Methods in Computational Physics*, *Vol. 9*; Alder, B., Fernbach, S., Rotenberg, M., Eds.; Academic Press: New York/London, 1970; Vol. 9, pp 135–211.
- (53) Darden, T.; York, D.; Pedersen, L. Particle Mesh Ewald: An N·log(N) Method for Ewald Sums in Large Systems. *J. Chem. Phys.* **1993**, *98* (12), 10089–10092.
- (54) Páll, S.; Hess, B. A Flexible Algorithm for Calculating Pair Interactions on SIMD Architectures. *Comput. Phys. Commun.* **2013**, *184* (12), 2641–2650.
- (55) Berendsen, H. J. C.; Postma, J. P. M.; Van Gunsteren, W. F.; Dinola, A.; Haak, J. R. Molecular Dynamics with Coupling to an External Bath. *J. Chem. Phys.* **1984**, *81* (8), 3684–3690.
- (56) Dequidt, A.; Devémy, J.; Malfreyt, P. Confined KCl Solution between Two Mica Surfaces: Equilibrium and Frictional Properties. *J. Phys. Chem. C* **2015**, *119* (38), 22080–

22085.

- (57) Heinz, H.; Koerner, H.; Anderson, K. L.; Vaia, R. A.; Farmer, B. L. Force Field for Mica-Type Silicates and Dynamics of Octadecylammonium Chains Grafted to Montmorillonite. *Chem. Mater.* **2005**, *17* (23), 5658–5669.
- (58) Daura, X.; Gademann, K.; Schäfer, H.; Jaun, B.; Seebach, D.; Van Gunsteren, W. F. The β-Peptide Hairpin in Solution: Conformational Study of a β-Hexapeptide in Methanol by NMR Spectroscopy and MD Simulation. *J. Am. Chem. Soc.* **2001**, *123* (10), 2393–2404.
- (59) Kabsch, W.; Sander, C. Dictionary of Protein Secondary Structure: Pattern Recognition of Hydrogen-bonded and Geometrical Features. *Biopolymers* **1983**, 22 (12), 2577–2637.
- (60) Touw, W. G.; Baakman, C.; Black, J.; Te Beek, T. A. H.; Krieger, E.; Joosten, R. P.; Vriend, G. A Series of PDB-Related Databanks for Everyday Needs. *Nucleic Acids Res.* 2015, 43 (D1), D364–D368.
- (61) Humphrey, W.; Dalke, A.; Schulten, K. VMD: Visual Molecular Dynamics. *J. Mol. Graph.* **1996**, *14* (1), 33–38.
- (62) Alcantar, N.; Israelachvili, J.; Boles, J. Forces and Ionic Transport between Mica Surfaces: Implications for Pressure Solution. *Geochim. Cosmochim. Acta* **2003**, *67* (7), 1289–1304.
- (63) Counterman, A. E.; Clemmer, D. E. Volumes of Individual Amino Acid Residues in Gas-Phase Peptide Ions. *J. Am. Chem. Soc.* **1999**, *121* (16), 4031–4039.
- (64) Wei, W.; Yu, J.; Gebbie, M. A.; Tan, Y.; Martinez Rodriguez, N. R.; Israelachvili, J. N.;

- Waite, J. H. Bridging Adhesion of Mussel-Inspired Peptides: Role of Charge, Chain Length, and Surface Type. *Langmuir* **2015**, *31* (3), 1105–1112.
- (65) Lu, Q.; Oh, D. X.; Lee, Y.; Jho, Y.; Hwang, D. S.; Zeng, H. Nanomechanics of Cation-π Interactions in Aqueous Solution. *Angew. Chemie Int. Ed.* **2013**, *52* (14), 3944–3948.
- (66) Chang, H.; Adibnia, V.; Li, C.; Su, R.; Qi, W.; Banquy, X. Short-Sequence Superadhesive Peptides with Topologically Enhanced Cation–π Interactions. *Chem. Mater.* 2021, 33 (13), 5168–5176.
- (67) Xiang, L.; Zhang, J.; Wang, W.; Gong, L.; Zhang, L.; Yan, B.; Zeng, H. Nanomechanics of π-Cation-π Interaction with Implications for Bio-Inspired Wet Adhesion. *Acta Biomater*. **2020**, *117*, 294–301.

Table of Contents Image:

